

Predictive response to the behaviour of old structures using ambient vibrations

Article Info:

Article history: Received 2024-05-06 / Accepted 2024-06-20 / Available online 2024-06-25

doi: 10.18540/jcecv10iss5pp19085



Zoubida Maraf

ORCID: <https://orcid.org/0000-0002-5974-9214>

Laboratory LCTPE, Department of Civil Engineering, University of Mostaganem, Algeria

E-mail: zoubida.maraf@univ-mosta.dz

Mounir Naili

ORCID: <https://orcid.org/0000-0003-4505-9738>

Laurentian University, Canada

E-mail: mnaili@laurentian.ca

Mohamed Bensoula

ORCID: <https://orcid.org/0000-0002-4785-3591>

Laboratory LCTPE, Department of Civil Engineering, University of Mostaganem, Algeria

E-mail: mohamed.bensoula@univ-mosta.dz

Abderrahmane Kibboua

ORCID: <https://orcid.org/0000-0002-7764-6884>

National Centre for Applied Research in Earthquake Engineering (CGS), Algiers, Algeria

E-mail: abderrahmane.kibboua@gmail.com

Hanifi Missoum

ORCID: <https://orcid.org/0000-0002-6306-6483>

Laboratory LCTPE, Department of Civil Engineering, University of Mostaganem, Algeria

E-mail: hanifimissoum@yahoo.fr

Abstract

The response of ancient structures such as the Saint-Jean-Baptiste church or the current El-Badr mosque in Mostaganem (Algeria) to earthquakes depends on these physical characteristics and consequently on modal properties such as frequencies, damping and modal deformations. In this paper, ambient vibration tests were carried out on the three parts of the mosque building, and the response spectra and damping obtained will be correlated with the mechanical tests carried out in the second part of the work. Determination of the dynamic characteristics made it possible to distinguish differences in stiffness and to clearly highlight a disparity in frequencies in each structure, which may correspond to the age of each part of the building, the design and construction and differences in levels, etc. The results of the destructive tests give indications that confirm the hypotheses of ageing of the materials. The low young modulus of the various components partly confirms the frequency and damping values obtained. The experimental study of the mosque using ambient vibrations will give an order of magnitude of the vibratory mode periods, which are the first steps in any modelling, reinforcement and/or verification strategy and constitute a health record for this type of heritage.

Keywords: Background noise, Mosque, Eigen modes, Frequency, Damping.

1. Introduction

Assessing the vulnerability of existing buildings by using seismic background noise recordings, which provide information on the actual dynamic behaviour of structures under low stress (Clotaire, 2007). The response of the structure to background noise (or ambient vibrations) is given in terms of modal frequencies, modal damping and modal deformations, and these three parameters constitute what are commonly known as the dynamic characteristics of the structure.

Many authors have considered the relevance of the use of ambient vibrations in the assessment of different structures, Dunand (2005) studied the building stock in Boumerdes damaged by the 2003 earthquake and the building stock in Grenoble and Nice, and emphasised the relevance of the seismic background noise for the dynamic characterisation and its contribution to the seismic diagnosis of earthquake-damaged structures. Ayad's contribution (2012) on monitoring the health of structures by choosing seismic background noise methods to define the dynamic characteristics of structures and their damage levels.

Limoge Schraen (2015) explored a method to diagnose the seismic vulnerability of a masonry church by integrating parameters derived from environmental vibration tests. Jetson A. Ronald and al (2018) modelled parts of a temple in India to extract the rate of its seismic vulnerability by integrating seismic background noise. Duco (2012) used in-situ ambient vibration tests on existing buildings to assess their rate of structural deterioration.

This measurement technique is well suited to ancient monuments, as the measured response is representative of the actual operating conditions of the structure, and is also considered to be non-destructive, inexpensive and significantly time-saving (on average 10 to 15 minutes per set of measurements) (El-Borgi, S. and al., 2008). This approach to vulnerability analysis was applied to the heritage of the city of Mostaganem in the case of the El-Badr mosque, where a background noise recording study was carried out to determine the modal characteristics of each structure, namely the old church, the sacristy and the minaret. The correlation between the parameters obtained by the test and the modulus of elasticity of each material extracted from the structures of the former church and sacristy, considered as an indicator of the mechanical performance of the building as a whole, will enable the results to be validated.

2. Experimentation

2-1 Presentation of the case study "the El-Badr mosque, former Saint Jean-Baptiste church"

The El Badr mosque is a former "Saint Jean-Baptiste" church, built between 1841 and 1848, located in the heart of the old colonial city of Mostaganem. with a cruciform plan that allows large openings, and has a central nave. The church was built in masonry (load-bearing walls) and consists of three rows of stone rubble, mostly sandstone, 65 cm thick and up to 70 cm wide. The quality of the rubble masonry is concealed by a natural portland cement CPN. The church was later extended around 1955 with a four-storey self-supporting sacristy. The floors are made of massive reinforced concrete slabs (20 cm thick) and the walls of masonry varying in thickness from 30 to 50 cm, due to the special ornamentation (crosses) on the four façades. The central part of the sacristy structure is grafted onto the old structure in the former choir, making it difficult to distinguish between the two. After independence, the church continued to be used as a Christian parish until 1980, when it was converted into a mosque, with some major alterations. The cruciform plan of the non-Muslim worship was eliminated, the bell tower was removed, and an addition of ablution room and sanitary in the north/north-west. The minaret, located in the north/north-east part of the building, have a self-supporting octagonal structure and reaches a height of 30.26 m.

The choice of this structure, also known as the "test building", was motivated by the difficulty of dealing with masonry and reinforced concrete structures from the last century in seismic

engineering, and by the difficulty of predicting their seismic behaviour. It is of particular interest because, like all the churches in Algeria, it has undergone several major modifications and deterioration over the years. It is made up of three different substructures, depending on the geometry, materials and structural system, as well as the dating of each substructure. We decoupled the parts of the structure that have very different modes and calibrated them with parameters specific to each substructure, before reassembling the whole structure using global calibration (Limoge, S. C., 2015).

2-2 Conduct and processing of ambient vibration measurements at the El-Badr mosque

The whole building was instrumented with several series of measurements because of the different blocks and the number of sensors (four Lennartz velocimeters three-component with the Cityshark II station, see supplementary material in Figure 1S and Figure 2S) (Benkaci, N. and al., 2021; Chatelain, J.L. and al., 2012; Kibboua, A., 2006; Kibboua, A. and al., 2008), cables are needed to complete the circuit with the recording station and a laptop for signal processing. Given the irregular shape of the structure, the arrangement of the sensors was designed to avoid redundancy and to illustrate the actual modes (Paquette, L.G., 2012).

For each recording, averaging 10 to 15 minutes (El-Borgi, S., 2008), the location of the fixed sensor used as reference was studied beforehand so as not to coincide with a node, i.e. a location that remains stationary while three mobile sensors or wick sensors are moved from one recording to another (Paquette, L.G., 2012). The seismometers represented by the abbreviations C1 to C13 have been positioned in the North-South direction indicated by NS, this direction follows the longitudinal direction of the building as shown in Figure 1.



Figure 1 - Location of the sensors on the structures.

Thus, the NS component corresponds to the longitudinal horizontal motion North-South, while the East-West direction indicated by the abbreviation EW corresponds to the transverse direction of horizontal movement and Z presents the vertical direction of mouvement (Chatelain, J.L. and al., 2012; Paquette, L.G., 2012).

In general, signal processing and identification is an important step in the whole monitoring process, because from the collected data, recordings can be made of each structure, whose natural frequencies, modal deformations and damping rates are relevant for determining the level of structural damage (Gattulli, V. and al., 2016). In order to resolve the non-stationary and random nature of the ambient vibrations, several modal exploration methods have been developed and integrated into data processing computer programs. The analyses of each data set were operated and performed with the Geopsy software (Benkaci, N. and al., 2021; Chatelain, J.L. and al., 2012) has integrated modules for calculating amplitude spectra using the fast Fourier transform. The singular value curves of spectral density matrices represent amplitude signals as a function of frequency or time. This amplitude can be a displacement, a velocity or an acceleration (Chatelain, J.L. and al., 2012). The modes are represented in three directions: vertical Z, longitudinal NS and transverse

EW. The damping coefficient of the eigen modes of the structure is estimated using the random decrement method (Gattulli, V. and al., 2016); Limoge, S. C., 2015), which is based on the principle of replicating a dynamic system to a random vibration and can be divided into two parts; the first corresponds to the impulse response of the system and the second to the forced response to the random stress.

The principle is based on removing the random component to reveal the impulse response by summing a large number of signal windows of the same initial value, for example zero displacement and positive velocity (Mikael, A., 2011), the random component of the response is then reduced compared to the impulse response, which has a zero mean at the end of the signal. From the impulse response it is easy to subtract the damping coefficient (ξ) (Kibboua, A. and al., 2008). In order to quantify the damage to the building materials used, such as the stone and concrete taken from the different sections; namely the prayer hall and the sacristy, we crushed the samples under destructive load in order to characterise the mechanical quantities.

3. Results of the experiment

The first modes recorded in each structure are shown in the response spectra recorded by the sensors, Figure 2 to Figure 14 shows all the singular spectral density curves for the three components for each sensor. Peak frequency values are obtained with one standard deviation within the interval bounded by two grey areas. The Table 1S to Table 14S shows estimates based on measurements of the natural frequencies and periods corresponding to the modes recorded for each sensor.

For the second part of the damping coefficient recording, the Table 1 to Table 19 and the Figure 3S to Figure 21S (in supplementary material) shows the damping coefficient (ξ) at each point for different frequency intervals (2 Hz to 12 Hz). The results of the destructive tests provide mechanical quantities such as the longitudinal modulus of elasticity of materials rock and concrete.

3-1 Determination of natural frequencies

The results of frequency show that there are several sharp peaks (the frequency peaks in the shaded columns have been selected as vibration modes) at a sampling frequency of 200 Hz, corresponding to a duration $\Delta t=0.005$ s between two recording points. Graphs A, B and C show the modes in the vertical Z, horizontal NS and EW directions respectively in the different sensors. The frequencies and amplitudes are indicated by the letters F and A respectively mentioned in the supplementary data.

Prayer hall (the former church): Due to the size of the prayer hall, the test was split into two recordings, the first; mezzanine represented by sensors C1 (reference sensor), C2 and C3 (wick sensors), and the second; priest's balcony represented by sensors C4 (reference sensor) and C5 (wick sensor).

Since it was not possible to place the collectors directly on the timbered roof, we placed them at mid-height (4.42 m for seismometers C2 and C3 and 5.43 m for the seismometer C5 as shown in Figure 1, which allows us to verify that the deformations measured on the roof follow the general trend of the building (Paquette, L.G., 2012), i.e. the vertical Z component at the top). The Figure 2 to Figure 4, and Table 1S to Table 3S (see supplementary material) shows the modal frequencies of the first recording in the prayer room:

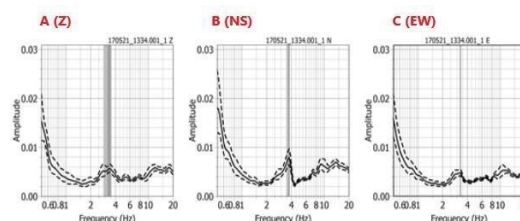


Figure 2 - Response spectrum of the signals recorded by the C1 sensor.

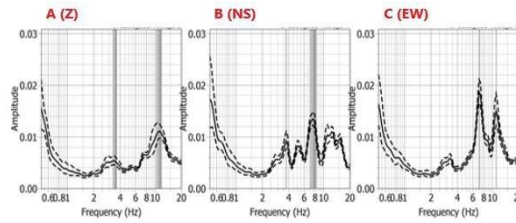


Figure 3 - Response spectrum of the signals recorded by the C2 sensor.

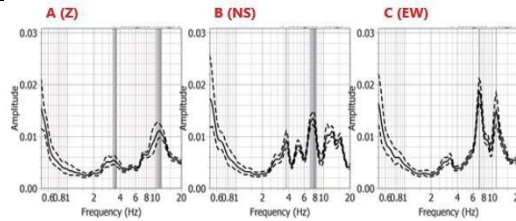


Figure 4 - Response spectrum of the signals recorded by the C3 sensor.

The Figure 5, Figure 6, and Table 4S to Table 5S (see supplementary material) shows the modal frequencies of the second recording in the prayer hall:

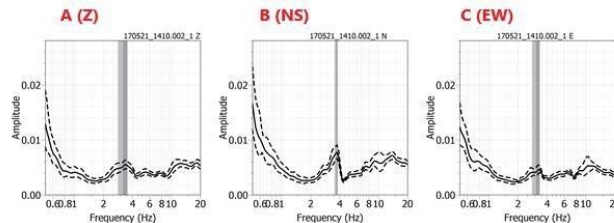


Figure 5 - Response spectrum of the signals recorded by the C4 sensor.

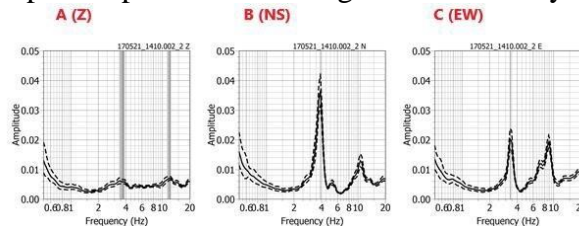


Figure 6 - Response spectrum of the signals recorded by the C5 sensor.

Sacristy: For the sacristy, the data are collected by seismometers C6, C7 and C9 (wick sensors), C8 (reference sensor), placed on each floor from the ground floor to the third floor as shown in Figure1. The Figure 7 to Figure 10, and Table 6S to Table 9S (see supplementary material) shows the modal frequencies of the recording in the sacristy:

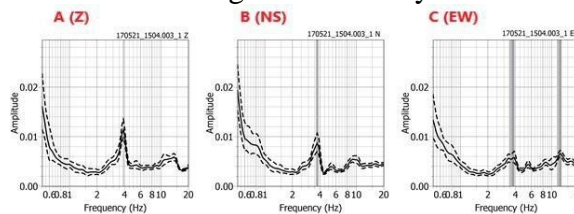


Figure 7 - Response spectrum of the signals recorded by the C6 sensor.

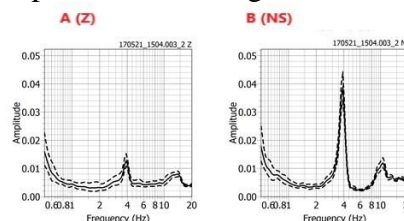


Figure 8 - Response spectrum of the signals recorded by the C7 sensor.

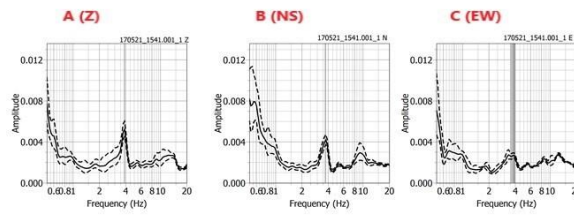


Figure 9 - Response spectrum of the signals recorded by the C8 sensor.

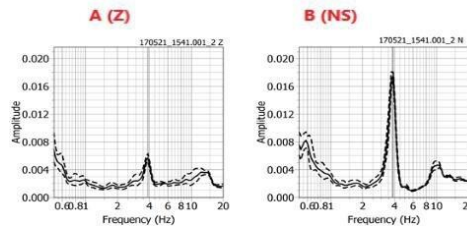


Figure 10 - Response spectrum of the signals recorded by the C9 sensor.

Minaret: For the minaret, the data set is obtained from seismometers C10, C12 and C13 (wick sensors), C11 (reference sensor), placed at the locations of each level from 0.3 m to 22.08 m as shown in Figure 1. The Figure 11 to Figure 14, and Table 10S to Table 13S (see supplementary material) shows the modal frequencies of the recording in the minaret:

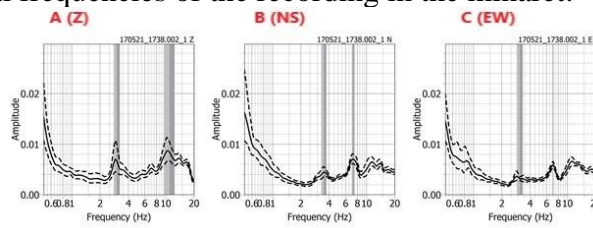


Figure 11 - Response spectrum of the signals recorded by the C10 sensor.

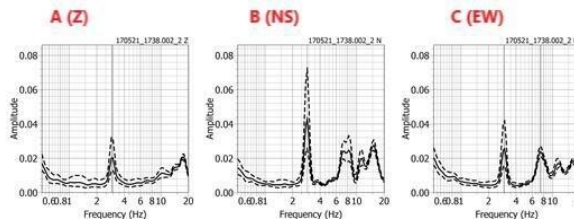


Figure 12 - Response spectrum of the signals recorded by the C11 sensor.

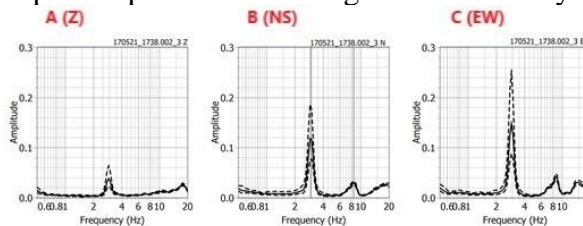


Figure 13 - Response spectrum of the signals recorded by the C12 sensor.

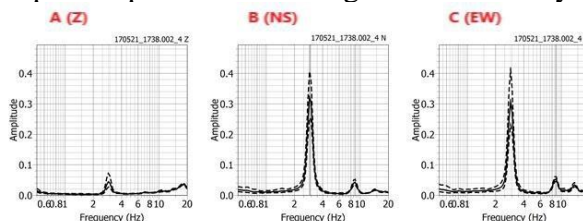


Figure 14 - Response spectrum of the signals recorded by the C13 sensor.

3-2 Determining the damping coefficient

The estimation of the values of the damping coefficient (ξ) of the eigen modes of El-Badr Mosque (the prayer hall, the sacristy and the minaret), by the signature of random decrement for each sensor in the different directions, the results are presented in the following figures and appendices.

Prayer hall: The Table 1 to Table 10 and Figure 3S to Figure 12S (see supplementary material) shows the values of the damping coefficient (ξ) of the prayer hall at the recording sensors C1 to C5:

Table 1 - Values of the damping coefficient at the recording point C1.

Directions	Frequencies / Hz	Damping / %
Vertical Z	3.4	7.22
Longitudinal NS	3.79	10.68
Transversal EW	3.38	4.08

Table 2 - Values of the damping coefficient between 2 Hz - 4 Hz at the recording point C2.

Directions	Frequencies / Hz	Damping / %
Vertical Z	3.29	9.50
Longitudinal NS	3.81	11.04
Transversal EW	3.39	2.86

Table 3 - Values of the damping coefficient between 6 Hz - 12 Hz at the recording point C2.

Directions	Frequencies / Hz	Damping / %
Vertical Z	10.22	7.37
Longitudinal NS	7.71	6.74
Transversal EW	9.25	23.15

Table 4 - Values of the damping coefficient between 2 Hz- 4 Hz at the recording point C3.

Directions	Frequencies / Hz	Damping / %
Vertical Z	3.26	9.99
Longitudinal NS	3.79	10.15
Transversal EW	3.41	3.28

Table 5 - Values of the damping coefficient between 4 Hz- 6 Hz at the recording point C3.

Directions	Frequencies / Hz	Damping / %
Vertical Z	5.25	5.69
Longitudinal NS	5.49	4.80
Transversal EW	5.63	7.99

Table 6 - Values of the damping coefficient between 6 Hz- 8 Hz at the recording point C3.

Directions	Frequencies / Hz	Damping / %
Vertical Z	7.22	2.41
Longitudinal NS	7.07	1.11
Transversal EW	7.27	2.52

Table 7 - Values of the damping coefficient between 8 Hz- 12 Hz at the recording point C3.

Directions	Frequencies / Hz	Damping / %
Vertical Z	10.26	5.53
Longitudinal NS	11	1.64
Transversal EW	10.62	3.94

Table 8 - Values of the damping coefficient at the recording point C4.

Directions	Frequencies / Hz	Damping / %
Vertical Z	3.43	7.17
Longitudinal NS	3.42	4.97
Transversal EW	3.39	2.94

Table 9 - Values of the damping coefficient between 2 Hz - 4 Hz at the recording point C5.

Directions	Frequencies / Hz	Damping / %
Vertical Z	3.43	4.16
Longitudinal NS	3.79	2.18
Transversal EW	3.43	0.46

Table 10 - Values of the damping coefficient between 8 Hz - 12 Hz at the recording point C5.

Directions	Frequencies / Hz	Damping / %
Vertical Z	10.54	4.31
Longitudinal NS	10.76	1.71
Transversal EW	8.90	1.78

Sacristy: For the sacristy, only two sensors recorded minimal (ξ) coefficient rates following the same frequency trend at the first floor and second floor levels. The Table 11 to Table 15 and Figure 13S to Figure 17S (see supplementary material) shows the values of the damping coefficient (ξ) of the sacristy at the recording sensors C6 to C9:

Table 11 - Values of the damping coefficient at the recording point C6.

Directions	Frequencies / Hz	Damping / %
Vertical Z	3.89	1.36
Longitudinal NS	3.85	1.47
Transversal EW	3.84	3.40

Table 12 - Values of the damping coefficient at the recording point C7.

Directions	Frequencies / Hz	Damping / %
Vertical Z	3.89	1.38
Longitudinal NS	3.88	0.94
Transversal EW	negligible value	negligible value

Table 13 - Values of the damping coefficient at the recording point C8.

Directions	Frequencies / Hz	Damping / %
Vertical Z	3.89	1.36
Longitudinal NS	3.87	1.63
Transversal EW	negligible value	negligible value

Table 14 - Values of the damping coefficient between 2 Hz-3 Hz at the recording point C9.

Directions	Frequencies / Hz	Damping / %
Vertical Z	2.88	0.87
Longitudinal NS	2.94	1.37
Transversal EW	2.89	1.06

Table 15 - Values of the damping coefficient between 3 Hz-4 Hz at the recording point C9.

Directions	Frequencies / Hz	Damping / %
Vertical Z	3.87	1.15
Longitudinal NS	3.87	0.94
Transversal EW	negligible value	negligible value

Minaret: The Table 16 to Table 19 and Figure 18S to Figure 21S (see Supplementary material) shows the values of the damping coefficient (ξ) of the minaret at the recording sensors C10 to C13:

Table 16. Values of the damping coefficient at the recording point C10.

Directions	Frequencies / Hz	Damping / %
Vertical Z	2.91	3.52
Longitudinal NS	3.34	8.23
Transversal EW	2.88	6.98

Table 17 - Values of the damping coefficient at the recording point C11.

Directions	Frequencies / Hz	Damping / %
Vertical Z	2.96	1.61
Longitudinal NS	2.87	0.31
Transversal EW	2.99	0.71

Table 18 - Values of the damping coefficient at the recording point C12.

Directions	Frequencies / Hz	Damping / %
Vertical Z	2.87	0.48
Longitudinal NS	2.95	1.26
Transversal EW	2.88	0.78

Table 19 - Values of the damping coefficient at the recording point C13.

Directions	Frequencies / Hz	Damping / %
Vertical Z	2.88	0.87
Longitudinal NS	2.94	1.37
Transversal EW	2.89	1.06

3-3 Determination of the modulus of longitudinal deformation by destructive tests

The results of the destructive tests allow us to deduce the Young's modulus indicated by the letter E for the sandstone rubble masonry of the prayer room E rock = 1457.49 MPa and for the reinforced concrete structure of the sacristy E concrete = 3206.34 MPa.

4. Analysis of results

4-1 Frequencies

It can be seen that the modal frequencies are heterogeneous and disparate depending on the type of structure being instrumented, which fall into two categories. The displacement oscillations highlight the modal components of the amplitudes, which are amplified at frequencies above 1 Hz; these are often the main modes that describe the dynamics of the structures in existing buildings, especially those with an ancient character such as ours. The frequencies are between 2.87 Hz and 12.07 Hz. They make up 59 vibration modes for the whole building, 28 modes for the prayer hall of the mosque, 11 modes for the sacristy and 20 modes for the minaret.

Prayer hall (former church): The prayer hall of the mosque has frequencies between 3.07 Hz and 11.85 Hz, the highest values are recorded in the vertical directions Z, NS and EW at the junction

between the prayer hall and the sacristy by the C5 sensor (11.85 Hz, 10.63 Hz and 8.81 Hz) (see Figure 6 and supplementary material in Table 5S), and at the junction between the prayer hall and the two structures of the minaret and the ablution room, recorded by the C2 and C3 sensors (7.11 Hz, 11.08 Hz, 5.14 Hz, 11.07 Hz, 7.61 Hz) (see Figure 3 and supplementary material in Table 2S) for the C2 sensor and (10.69 Hz, 5.18 Hz, 7.11 Hz, 7.59 Hz, 11.05 Hz and 11.16 Hz) (see Figure 4 and supplementary material in Table 3S) for the C3 sensor, these values significantly exceed the frequencies recorded by the reference sensors placed on the ground (C1 and C4) (see Figure 2, Figure 5 and supplementary material in Table 1S, Table 4S).

The significant difference in the frequency values can be explained by the difference in the stiffness and mass at which the measurement points were taken, and means that the points of connection between the different structures with that of the prayer hall constitute a blockage created by the reinforced concrete side structures built at a later date on the north and south sides therefore have low rigidity and natural periods, justifying minimal displacement.

Also, the majority of the modal deformations are torsion-flexion, influenced by the horizontal geometric irregularities (the original shape of former church in the form of a cross on which a sacristy was grafted and finally used for religious purposes, the cross was removed after the building was converted in 1980, with the addition of two 5 m high blocks for the ablution room and the base covering the minaret, which rises to 30.26 m, resulting in uneven bending along the entire length of the prayer hall).

In most of the sensors (C1, mode 2 of C3, C4, C5) (see Figure 2, Figure 4 to Figure 6 and supplementary material in Table 1S, Table 3S to Table 5S), the frequencies of the prayer hall in the NS directions are higher than those in the EW direction, which explains why there is a greater stiffness in the longitudinal direction (Mikael, A., 2011); in fact, the particular characteristics of Christian religious buildings, is that the two side walls with timid openings of a Romanesque design are characterised by a squat architecture and a low slenderness of the load-bearing walls, with a thickness of 65 cm to 70 cm resting on a string of arches highlighting the central nave, and makes the side walls more flexible than the North and South fronts. It is also the effectiveness of this connection that causes the torsional component of the bending mode (Chabane, S. and al., 2019; Kibboua, A. and al., 2008), so in terms of displacement this remains minimal. These explanations can be also linked to the random decrement method, which can increase the values of one direction relative to another.

Sacristy: The sacristy has the lowest frequencies, ranging from 3.65 Hz to 12.07 Hz. The building has a certain symmetry in plan and elevation, except in a few places, such as the location of the staircase on the south-south/west side on the ground floor, which goes from the second floor to the north-north/west, and the presence of a balcony in the third floor in the choir hall, creating a double height of more than 5 m for this floor. This explains the slight difference in the frequency values of the vertical Z components (3.88 Hz for the C6 and C7 sensors) (see Figure 7, Figure 8 and supplementary material in Table 6S, Table 7S), and (3.86 Hz for the C8 and C9 sensors) (see Figure 9, Figure 10 and supplementary material in Table 8S, Table 9S).

The same applies to the values of the horizontal longitudinal components NS, where we see 3.72 Hz at the C6 sensor (see Figure 7 and supplementary material in Table 6S), 3.88 Hz at the C7 sensor (see Figure 8 and supplementary material in Table 7S), 3.71 Hz at the C8 sensor (see Figure 9 and supplementary material in Table 8S), and 3.83 Hz at the C9 sensor (see Figure 10 and supplementary material in Table 9S).

For the horizontal transverse component EW, two recordings of 3.65 Hz and a frequency peak of 12.07 Hz at the C6 sensor (see Figure 7 and supplementary material in Table 6S) and the value of 3.75 Hz at the C8 sensor (see Figure 9 and supplementary material in Table 8S), very low or even negligible amplitude and frequency values were observed for the C7 and C9 sensors (see Figure 8, Figure 10 and supplementary material in Table 7S, Table 9S).

The minimal difference between the frequency values of the two longitudinal components NS and EW can be explained by the symmetrical layout of the spaces and the ascending lightening of

the partitions in the distribution of the rooms: the higher you go, the more pronounced the decompartmentalization until you reach the choir hall with an open balcony.

It can also be seen that the frequencies in the NS direction (3.72 Hz, 3.88 Hz, 3.71 Hz and 3.83 Hz) are slightly higher than those in the other EW direction (3.65 Hz and 3.75 Hz) (see supplementary material in Table 6S to Table 9S), which indicates the stiffness in the NS direction (Mikael, A., 2011) due to the interlocking with the masonry walls of the mosque as well as the greater number of walls in this direction, the transverse EW component is free of blocking and leads to the majority of the modal deformations in torsional bending.

The frequency peak of 12.07 Hz recorded at the C6 sensor (see Figure 7 and supplementary material in Table 6S) means that the location of the sensor adjacent to one of the load bearing masonry walls of the prayer hall and its position close to the reinforced concrete staircase located at the south/southwest corner influences on the spectral response and the stiffness of the structure.

Minaret: For the minaret, which has heterogeneous frequencies oscillating around 2.88 Hz to 3.52 Hz and other values around 7.01 Hz to 8.79 Hz with a significant peak recorded in the first C10 sensor in the direction of the vertical Z component at a value of 11 Hz (see Figure 11 and supplementary material in Table 10S).

The frequency values of the first three modes are very far from the last modes in each sensor (3.01 Hz, 3.52 Hz and 3.11 Hz) for the first low values and (11 Hz, 7.17 Hz and 7.01 Hz) for the higher values in the C10 sensor (see Figure 11 and supplementary material in Table 10S), the low values of 2.94 Hz, 2.88 Hz and 2.96 Hz and the high value of 7.38 Hz for the C11 sensor (see Figure 12 and supplementary material in Table 11S), low values of 2.88 Hz and 2.94 Hz and high values of 8.39 Hz and 8.49 Hz for the C12 sensor (see Figure 13 and supplementary material in Table 12S), low values of 2.88 Hz and 2.91 Hz and two high values of 8.79 Hz and 8.76 Hz for the C13 sensor (see Figure 14 and supplementary material in Table 13S).

The minaret has a symmetrical octagonal configuration, so the mode shapes have the same dynamic properties in both horizontal directions (NS and EW) (Khaldoon, B.H. and al., 2008). This similarity in frequency values in both directions (see supplementary data in Table S10 to Table S13) gives rise to modal deformations (mode shapes) in torsion-flexion (Khaldoon, B.H. and al., 2008). Similarly, the absence of pronounced irregularities in elevation allows the existence of much more regular bending modes (Paquette, L.G., 2012).

The value of the 11 Hz peak (see Figure 11 and supplementary data in Table S10) suggests an increase in stiffness due to the interconnection between the base of the minaret and the rest of the prayer hall structure.

4-2 Damping

The wide distribution of damping coefficients refers to parameters intrinsic to each structure's ability to dissipate energy (Dunand, F., 2005), as well as to other external factors.

The prayer hall: In the prayer hall, for different frequency ranges from 2 Hz to 12 Hz, low damping coefficients between 1.11% and 4.80% were reported for some sensors and high coefficients between 7.22% and 11.04% for others, except for the C2 sensor with a very high rate of 23.15%, which makes no physical sense, most of these values are generally very low compared to those used in calculations for masonry structures, between (7% - 10%) (Kibboua, A., 2006).

Sacristy: For the sacristy, very low damping coefficients were reported for different frequency ranges from 2 Hz to 4 Hz, varying between 0.94% and 3.40%, and in some cases even negligible, especially in the horizontal EW direction, bearing in mind that most of these values are very low compared to those used in calculations for reinforced concrete structures, generally between (5% - 7%) (Kibboua, A., 2006).

Minaret: For the minaret, and for the various frequency ranges from 2 Hz to 4 Hz, very low to low damping rates are reported, ranging from 0.31% to 3.52% for some sensors, and damping values within the range of recommendations for this type of structure ranging from 6.98% to 8.23% recorded in the C10 sensor (see Table 16 and supplementary material in Figure 18S).

The structures tested show different rates of deterioration due to various factors specific to the buildings and other external factors, and it is impossible to justify each structure in isolation from the others. During the site visits, we noted many anomalies due to the passage of time, the use of the buildings and their neglect. The connections between the different types of walls (load-bearing and infill), the heterogeneity of the materials, their aging-fatigue cycles and the internal friction in the different structures affect the ability to absorb and dissipate energy, and the mobilisation of imperfections, triggers damping in the structures (Mikael, A., 2011).

The absence of a joint at the junction of each structure with the parent structure (the prayer hall) creates a visible overlap, giving rise to fears of hammering problems on the north and south flanks of the intital structure, leading to cracks. This phenomenon, to which unreinforced masonry is highly susceptible (Aşikoğlu, A., 2018; Paquette, L.G., 2012), may also explain the high damping values at some sensors. These cracks, mainly the hidden or invisible ones, bear tiny changes in frequency but up to 50% for the damping coefficient (Mikael, A., 2011). This was noticeable at the C2 and C3 sensors (see Table 2 to Table 7 and supplementary material in Figure 4S to Figure 9S), the C8 sensor (EW component) (see Table 13 and supplementary material in Figure 15S), and the C10 sensor (see Table 16 and supplementary material in Figure 18S).

All the bibliographical references mention that the damping depends on the frequencies, whatever the ground (Dunand, F., 2005; Mikael, A., 2011). By analysing the damping values with those of the frequencies, for the prayer hall; an increase in the coefficients with the frequencies at the level of the C1 sensor in the EW direction (see Table 1 and supplementary material in Figure 3S), the C2 sensor between 2 Hz - 4 Hz in the vertical Z and horizontal EW directions (see Table 2 and supplementary material in to Figure 4S), between 6 Hz - 12 Hz for all directions (see Table 3 and supplementary material in to Figure 5S), with a significant increase in the damping reaching 23.15% for the EW component, for the C3 sensor, between 2 Hz - 4 Hz in the vertical Z and horizontal EW directions (see Table 4 and supplementary material in to Figure 6S), between 4 Hz - 6 Hz in all directions (see Table 5 and supplementary material in to Figure 7S), between 8 Hz - 12 Hz in the vertical Z direction (see Table 7 and supplementary material in to Figure 9S), for the C4 sensor, in all directions (see Table 8 and supplementary material in to Figure S10).

Or, the decrease of the coefficient is observed with the increase of the frequencies in certain directions of the C2 sensors, between 2 Hz - 4 Hz in the horizontal direction EW (see Table 2 and supplementary material in to Figure 4S), of the C3 sensor, between 6 Hz - 8 Hz in all directions (see Table 6 and supplementary material in to Figure 8S), between 8 Hz - 12 Hz in the horizontal directions NS and EW (see Table 7, supplementary material in to Figure 9S), and for the C5 sensor, between 2 Hz - 4 Hz in the horizontal directions NS and EW (see Table 9 and supplementary material in to Figure 11S), where even the lowest coefficient of 0.46% in the EW direction, between 8 Hz-12 Hz in all directions (see Table 10 and supplementary material in to Figure 12S). These sensors are located in the upper part of the hall and their values are justified by the movement that can be generated by the wooden framework, which has its own response and influences the values of the mentioned sensors.

For the sacristy, almost all the values of the damping coefficients do not follow the same pattern as the frequencies, which oscillate between 2.88Hz and 3.89Hz. As far as the coefficients are concerned, they remain around 0.87% to 1.63%, except for the maximum value of 3.4% at the level of the EW component of sensor C6 (see Table 11 and supplementary material in to Figure 13S), at the level of the C9 sensor, between 2Hz and 3Hz, a decrease in frequencies and damping is recorded in all directions compared to the other sensors (see Table 14 and supplementary material in to Figure 16S).

For the minaret, the damping values follow the trend of the frequency values for most of the sensors in the interval 2.87 Hz and 3.34 Hz with coefficient variations between 0.31% and 3.52%, except for the C10 sensor where there is an increase in damping without frequency in the horizontal directions NS of 8.23% and EW of 6.98% (see Table 16 and supplementary material in to Figure 18S).

As mentioned in the presentation of the project, the Church of Saint Jean-Baptist was converted to the mosque, in order to provide access to the ablution room, one of its connections, i.e. the north/north-west edge of the building was removed and the arch was condemned by filling it in with masonry.

For the purpose of the worshippers' ablutions, a depth of 70 cm and dimensions of 1.70 m long by 0.54 m wide perforation was made in the north/northwest bearing wall to access the water tank, which means that the destruction of the walls contributed to the rigidity of the structure in this direction [17] at the level of the nearest C3 sensor (see Table 4 to Table 7 and supplementary material in to Figure 6S to Figure 9S).

This patrimonialization can contribute significantly to the spectral response of the building [19] and can create a difference in stiffness and cause the frequency to drop by up to 8% (Dunand, F., 2005; Mikael, A., 2011).

The movements of the building generate waves that propagate in the ground, diverging from the point of emission, which is also considered as damping (Dunand, F. and al., 2002). This damping is attenuated by the frequency of the building and the stiffness of the foundation soil (Kibboua, A., 2006); damping is high in soft soils and low in hard or stiff soils. According to the geological area of Mostaganem region, the site is composed of Lumachian limestone sandstone covered by a Quaternary limestone shell. The whole is masked by alluvium and sand attributed to the Quaternary [8], this first layer, being less rigid, can generate the phenomenon of soil-structure interaction, and a classification according to Algerian parasismic regulation 2003 (RPA 2003) can be assigned to soil being firm with a velocity indicated by $VS \geq 400$ m/s and < 800 m/s (CGS, 2003).

Seismic episodes that affect the city of Mostaganem, classified according to the RPA 2003 in zone II-a with a seismic zoning that gives rock accelerations of 0.15g for a return period of 100 years (CGS, 2015), can lead to a loss of stiffness in the building stock and can cause frequencies to decrease by 10% to 40% (Dunand, F., 2005; Mikael, A., 2011). It should be noted that no measurements of modal characteristics have been made for the building, so we can in no way assume that frequencies have decreased because of previous earthquakes.

The damping values and frequencies are also justified by other parameters such as the number of storeys, the prayer hall, which extends over a height of 5.60 m on the aisles and culminates at a height of over 13 m, leaving a central nave at a height of 11 m, the sacristy, which is built over 4 storeys with a total height of over 20 m, and the minaret, which culminates at a height of over 30 m due to its function.

Changes in the frequency values of up to 5% are not directly related to damage to the structure. This may be due to climatic variations such as temperature and humidity (Mikael, A., 2011). Winds do not follow the same trend as temperature: as the wind amplitude increases, the frequency decreases. It has been observed that, at moderate levels of stress, it can lead to the opening and closing of pre-existing cracks, thereby reducing stiffness and therefore frequency. This level of excitation is comparable to small seismic shocks (Mikael, A., 2011). On the day of the measurements, we recorded an average temperature between 20°C and 27°C and a relatively low wind speed of 26 km/h (Historique-meteo.net, 2017). No precipitation was recorded, so the long-term monitoring of climatic variations and their impact on the building was not investigated in this article.

The presence of an underground water reservoir can have the same effect as rainfall that saturates the soil, which can lead to differences in behaviour over a short distance is 0.52 m from the foundations of the north/north-west load bearing wall and has never been maintained, had been never control from water leakage and is therefore likely to saturate the soil surrounding the load bearing foundations in this direction and introduce damping values.

We have seen that frequencies and damping are largely dependent on the same phenomena and respond to the same consequences (Dunand, F., 2005). However, it has been observed that two climatic factors significantly affect the response of the structure, namely temperature and precipitation, leading to an increase in frequency.

4-3 Longitudinal modulus of deformation

For simple or known structures, only a few parameters are involved in the dynamic behaviour. In general, the main unknown comes from the state of degradation of the constituent materials (Augenti, N. and Fluvio, P., 2011; Chaibedra, B. and al., 2017; Gharib, T., 2015; Mikael, A., 2011). To complete this study, we correlated the first experiment with mechanical tests which indicate that the Young's modulus values are much lower ($E_{\text{rock}} = 1457.49 \text{ MPa}$, $E_{\text{concrete}} = 3206.34 \text{ MPa}$) than those in the literature (Afnor, 1999; Ambroziak, A. and al., 2019; Kaushik, H. and al., 2007; Mikael, A., 2011; Sohail, M. G. and al., 2018). This explains the various degradations observed as these materials deteriorated and aged over time.

5. Conclusion

A summary of the results of the ambient vibration tests carried out on the El-Badr mosque was presented, allowing a more accurate assessment of the existence of the modes identified in the various structures subjected to the test. Once the data had been collected, a computer programme was used to process the information, extracting and interpreting the signals recorded using the inverse Fourier transform to extract the main vibration modes, i.e. the natural frequencies and damping using the random decrement method.

The modal frequencies and damping rates are heterogeneous and different according to the type of structure. By comparing them with the values derived from the international bibliography, we find an underestimation of the frequencies (Dunand, F. and al., 2002) and of the calculated damping (reinforced concrete structures (5%-7%) and masonry structures (7%-10%)) (Dunand, F. 2005; Kibboua, A., 2006).

These results make it difficult to interpret the variations and do not allow us to clearly identify modes specific to each structure, since the variables between the different structures are significant and contribute to the heterogeneity of these data.

To support these conclusions, the scientific community agrees on the influence of certain parameters that group the two categories of structure together:

- The prayer hall of the mosque (ex-church) in load-bearing masonry, the sacristy and minaret in a self-stable reinforced concrete structure, the whole forming a complex monobloc in materials, the differences in stiffness of each structural system and in relation to the complex shapes in plan and mass (Paquette, L.G., 2012).

- The embedding of the structures, the geometry and position of the building in the block (head, corner, middle) and the variations in gauge of one structure to another would not have the same frequencies (Douiri, A. and al., 2015), and damage and degradation of structures, soil-structure interaction. Age, and consequently the poor quality of materials and their fatigue (Jeston, A. R. and al., 2018), the rate of degradation of buildings during their life is also a major issue in frequency variations (Aldea, A. and al., 2018).

- The numerous cracks observed and various rehabilitations or previous works (removals and additions) reduce the overall stiffness of the building.

- The effect of the flexibility of the facades, especially for the sacristy with the distribution of window and door openings, influences the shapes of the main modes (Aşikoğlu, A., 2018).

- Other causes can be cited as disturbances of the test such as heat, sensitive recording equipment, and assembly and disassembly cycles can also affect the recording (Mikael, A., 2011).

- The mechanical quantities obtained from the destructive tests show weaknesses in the longitudinal deformation moduli for rock and concrete and justifies the results obtained from the non-destructive tests in terms of frequencies and damping coefficients.

This ambient vibration monitoring campaign allowed us to determine the condition of the El-Badr mosque, to assess the feasibility of measuring in heritage buildings, to locate the frequency register of this type of structure and then to observe the shapes of the main modes. They provide

information on the state of loss of stiffness and/or the degree of vulnerability of the whole building and can be used for strengthening purposes in the event of new earthquakes.

5. Supplementary Material

The supplementary materials contain the equipment used for background noise (station and sensor), the modal frequency values and amplitude peaks identified in each sensor, and the damping curves in each sensor.

The free access to the supplementary material at jCEC website

Acknowledgements

The authors would like to express their sincere thanks to their colleagues at the National Centre for Applied Research in Earthquake Engineering, Algiers, Algeria, for using their ambient vibration equipment.

The authors report there are no competing interests to declare.

References

- Afnor 1999). *Methods of testing masonry - Part 1: Determination of compressive strength" (Méthodes d'essai de la maçonnerie - Partie 1: détermination de la résistance à la compression)*. National standards and national normative documents, Afnor Editions, France.
- Aldea, A.; Neagu, C.; Lozinca, E.; Demetriu, S.; Bourdim, S.M.E.A and Turano, F. (2018). Toward the Seismic Evaluation of Caro 1 Royal Mosque in Constanța. Seismic Hazard and Risk Assessment: Updated Overview with Emphasis on Romania. *Springer international publishing*.
https://doi.org/10.1007/978-3-319-74724-8_23
- Ambroziak, A.; Haustein, E.; Kondrat, J. (2019). Chemical and mechanical properties of 70-year-old concrete. *Journal of materials in civil engineering* 31.8.
[https://doi.org/10.1061/\(ASCE\)MT.1943-5533.000284](https://doi.org/10.1061/(ASCE)MT.1943-5533.000284)
- Aşikoğlu, A. (2018). *Numerical investigation on the effectiveness of seismic retrofitting of a historical masonry mosque*. Master of science thesis, Anadolu University, Turkey.
<https://www.proquest.com/openview/2b96d1ef67b884968ddfc5d0c2cdec36/1?pq-origsite=gscholar&cbl=2026366&diss=y> , consulted on 10/03/2020
- Augenti, N., and Fulvio P. (2011). Constitutive modelling of tuff masonry in direct shear. *Construction and building materials* 25.4, 1612-1620.
<https://doi.org/10.1016/j.conbuildmat.2010.10.002>
- Ayad, M. (2012). *Monitoring the health of structures (Control de la santé des structures)*. Master's thesis, Abou Bakr Belkaid University, Tlemcen, Algeria. <http://dspace1.univ-tlemcen.dz/handle/112/3081> , consulted on 02/01/2024
- Benkaci, N.; Oubaiche, E.H.; Châtelain, J.L.; Bensalem, R; Benouar, D and Abbès, K. (2021). Non-stability and non-reproducibility of ambient vibration HVSR peaks in Algiers (Algeria). *Journal of earthquake engineering* 25.5: 853-871.
<https://doi.org/10.1080/13632469.2018.1537903>
- Chabane, S.; Bezzeghoud, M.; Fontiela, J.; Machane, D.; Oubaiche, E.H. and Bensalem, R. (2019). Site effect in Algiers area, Algeria, workshop em ciencias da terra e do espaço, Universidade de Evora, Spain. <https://www.researchgate.net/publication/330936982> , consulted on 06/05/2023
- Chaibedra, B.; Benanane, A. and Boutaraa, Z. (2017). Numerical multi-modeling and seismic analysis of historical URM building. *Asian journal of civil engineering (BHRC)* 18.8: 1341-1351. <https://www.researchgate.net/publication/319620763> , consulted on: 17/04/2019

- Chatelain, J.L.; Guillier, B; Guéguen, P; Fréchet, J and Sarrault, J. (2012). Ambient vibration recording for single-station, array and building studies made simple: *CityShark II. International journal of geosciences* 3: 1168-1175. <https://doi.org/10.4236/ijg.2012.326118>
- CGS (2003). *Algerian seismic regulations 2003 version (Règlement parasismique algérien version 2003)*. Regulatory technical document, CGS, Algiers, Algeria.
- CGS (2015). *Regional study of the seismic hazard in the wilaya of Mostaganem (Etude régionale de l'aléa sismique des wilaya de Mostaganem)*. Final report (stage 7), CGS, Algiers, Algeria.
- Clotaire, M. and Guéguen, P. (2007). Large-scale seismic vulnerability analysis using experimental dynamic properties of buildings (Analyse de vulnérabilité sismique à grande échelle par utilisation des propriétés dynamiques expérimentales des bâtiments), 7th National Symposium AFPS. <https://arxiv.org/ftp/arxiv/papers/0710/0710.1603.pdf> , consulted on 26/03/2021
- Douiri, A.; Mourabit, T.; Cheddadi, A.; Chourak, M and Louhibi, S. (2015). Spectral coincidences of background noise between soil and existing buildings in Imzouren city, Morocco. *Journal of materials and environmental science*: 366-376. <http://brujula.ual.es/publications/84177> , consulted on 14/02/2023
- Duco, F. (2012). *Methodologies for assessing the seismic vulnerability of existing buildings using in situ instrumentation (méthodologies d'évaluation de la vulnérabilité sismique de bâtiments existants à partir d'une instrumentation in situ)*. Doctoral thesis, National Polytechnic Institute of Toulouse, France. <https://theses.hal.science/tel-04244976v1/document> , consulted on: 05/06/2022
- Dunand, F.; Bard, P.Y.; Chatelain, J.L.; Guéguen, P.; Vassail.T. Thierry. (2002). Damping and frequency from Randomdec method applied to in situ measurements of ambient vibrations. Evidence for effective soil structure interaction, 12th European conference on earthquake engineering, London. Paper. Vol. 869. <https://www.researchgate.net/publication/350836822>, consulted on 14/10/2022
- Dunand, F. (2005). *Relevance of seismic background noise for dynamic characterisation and seismic diagnosis of civil engineering structure (Pertinence du bruit de fond sismique pour la caractérisation dynamique et l'aide au diagnostic sismique des structures de génie- civil)*. Doctoral thesis, Joseph-Fourier-Grenoble I, France. <https://theses.hal.science/tel-00335885> , consulted on 14/03/2021
- El-Borgi, S.; Choura, S; Neifar, M; Smaoui, H; Majdoub, M.S and Cherif, D. (2008). Seismic vulnerability assessment of a historical building in Tunisia. *Smart structures and systems an international journal* 4.2: 209-220. <https://doi.org/10.12989/sss.2008.4.2.209>
- Gattulli, V.; Marco L. and Francesco P. (2016). Dynamic testing and health monitoring of historic and modern civil structures in Italy. *Structural Monitoring and Maintenance* 3.1. <https://doi.org/10.12989/smm.2016.3.1.071>
- Gharib, T. (2015). *Reinforcement of historic masonry structures using composite materials: application to limestone walls (Renforcement des structures historiques en maçonnerie par matériaux composites: application aux murs en pierres calcaires)*. Doctoral thesis, Claude Bernard University, Lyon 1, France. <https://theses.hal.science/tel-01186203> , consulted on 14/08/2018
- Historique-meteo.net. <https://www.historique-meteo.net/afrique/algerie/mostaganem/2017/05/17/>, consulted on 29/05/2020.
- Jeston, A. R.; Menon, A.; Meher, P. A.; Menon, D.; Magenes, G. (2018). Modelling and analysis of South Indian temple structures under earthquake loading. *Sādhanā*, 43, 74. <https://doi.org/10.1007/s12046-018-0831-0>
- Kaushik, H.; Rai, D. and Jain, S. K. (2007). Stress-strain characteristics of clay brick masonry under uniaxial compression. *Journal of materials in civil engineering* 19.9: 728-739. [http://dx.doi.org/10.1061/\(ASCE\)0899-1561\(2007\)19:9\(728\)](http://dx.doi.org/10.1061/(ASCE)0899-1561(2007)19:9(728))
- Khaldoon, B.H.; Zibdeh, H. and Hamdaoui, K. (2008). Health monitoring of a historical monument in Jordan based on ambient vibration test. *Smart structures and systems* 4. 195-208.

- <https://doi.org/10.12989/sss.2008.4.2.195>
- Kibboua, A. (2006). *Dynamic study under ambient vibrations of a cable-stayed bridge over the Oued Dib in Mila (Etude dynamique sous vibrations ambiantes d'un pont à haubans sur l'Oued Dib à Mila)*. Doctoral thesis, National School of Public Works, Algiers, Algeria. <https://www.researchgate.net/publication/324529261>, consulted on 05/07/2022.
- Kibboua, A.; Farsi, M.N.; Chatelain, J.L.; Guillier, B.; Bechtoula, H. and Mehani, Y. (2008). Modal analysis and ambient vibration measurements on Mila-Algeria cable stayed bridge. *Structural engineering and mechanics* 29.2:171-186. <https://doi.org/10.12989/sem.2008.29.2.171>
- Limoge, S. C. (2015). Towards a large-scale seismic vulnerability diagnostic method for historical heritage (Vers une méthode de diagnostic de vulnérabilité sismique à grande échelle pour le patrimoine historique). *Rencontres universitaires de génie civil*. <https://hal.science/hal-01167608>, consulted on 16/08/2019.
- Mikael, A. (2011). *Evaluation of the physical parameters of buildings: damping, frequency and modes of behaviour of civil engineering structures - Experimental approach (Evaluation des paramètres physiques des bâtiments: amortissement, fréquence et modes de comportement des structures de génie civil- Approche expérimentale)*. Doctoral thesis, Grenoble University, France. <https://theses.hal.science/tel-00597269>, consulted on 12/12/2023
- Paquette, L.G. (2012). *Characterisation of buildings with unreinforced masonry and their dynamic properties (Caractérisation des bâtiments comprenant de la maçonnerie non renforcée et de leurs propriétés dynamiques)*. Master's thesis, Sherbrooke University, Canada. <http://savoirs.usherbrooke.ca/handle/11143/1621>, consulted on 10/02/2023.
- Sohail, M. G.; Kahraman, R.; Ozerkan, G.; Alnuaimi, N.; Gencturk, B., Belarbi, A. and Dawood, M. (2018). Reinforced concrete degradation in the harsh climates of the Arabian Gulf: field study on 30-to-50-year-old structures. *Journal of performance of constructed, facilities* 32.5 04018059. [https://doi.org/10.1061/\(ASCE\)CF.1943-5509.0001204](https://doi.org/10.1061/(ASCE)CF.1943-5509.0001204)

Supplementary Material:



Figure 1S. Station used for background noise.



Figure 2S - Sensor used for background noise.

Table 1S- Modals frequencies and amplitudes peaks identified for the sensor C1.

Mode	Frequencies / Hz	Amplitude peak	Directions
1	3.19	0.00538	Vertical Z
2	3.66	0.0077	Longitudinal NS
3	3.28	0.0048	Transversal EW

Table 2S - Modals frequencies and amplitudes peaks identified for the sensor C2.

Mode	Frequencies / Hz	Amplitude peaks	Directions
1	3.47	0.0053	Vertical Z
2	3.73	0.009	Longitudinal NS
3	7.11	0.0186	Transversal EW
4	11.08	0.011	Vertical Z
5	5.14	0.0082	Longitudinal NS
6	11.07	0.0149	Transversal EW
7	7.61	0.0135	Longitudinal NS

Table 3S- Modals frequencies and amplitudes peaks identified for the sensor C3.

Mode	Frequencies / Hz	Amplitude peaks	Directions
1	3.49	0.005	Vertical Z
2	3.72	0.0088	Longitudinal NS
3	3.08	0.006	Transversal EW
4	10.69	0.010	Vertical Z
5	5.18	0.008	Longitudinal NS
6	7.11	0.0226	Transversal EW
7	7.59	0.014	Longitudinal NS
8	11.05	0.0174	Transversal EW
9	11.16	0.0105	Longitudinal NS

Table 4S- Modals frequencies and amplitudes peaks identified for the sensor C4.

Mode	Frequencies / Hz	Amplitude peaks	Directions
1	3.18	0.0052	Vertical Z
2	3.67	0.0077	Longitudinal NS
3	3.07	0.0042	Transversal EW

Table 5S- Modals frequencies and amplitudes peaks identified for the sensor C5.

Mode	Frequencies / Hz	Amplitude peaks	Directions
1	3.62	0.0059	Vertical Z
2	3.88	0.036	Longitudinal NS
3	3.36	0.0202	Transversal EW
4	11.85	0.0071	Vertical Z
5	10.63	0.013	longitudinal NS
6	8.81	0.019	Transversal EW

Table 6S- Modals frequencies and amplitudes peaks identified for the sensor C6.

Mode	Frequencies / Hz	Amplitude	Directions
1	3.88	0.01143	Vertical Z
2	3.72	0.0086	Longitudinal NS
3	3.65	0.0055	Transversal EW
4	12.07	0.0064	Transversal EW

Table 7S- Modals frequencies and amplitudes peaks identified for the sensor C7.

Mode	Frequencies / Hz	Amplitude peaks	Directions
1	3.88	0.0128	Vertical Z
2	3.88	0.0385	Longitudinal NS
3	Negligible values in transversal EW direction		

Table 8S- Modals frequencies and amplitudes peaks identified for the sensor C8.

Mode	Frequencies / Hz	Amplitude peaks	Directions
1	3.86	0.0052	Vertical Z
2	3.71	0.0041	Longitudinal NS
3	3.75	0.0055	Transversal EW

Table 9S- Modals frequencies and amplitudes peaks identified for the sensor C9.

Mode	Frequencies / Hz	Amplitude peaks	Directions
1	3.86 Hz	0.0057	Vertical Z
2	3.83 Hz	0.0173	Longitudinal NS
3	Negligible values in transversal EW direction		

Table 10S- Modals frequencies and amplitudes peaks identified for the sensor C10.

Mode	Frequencies / Hz	Amplitude peaks	Directions
1	3.01	0.0066	Vertical Z
2	3.52	0.0044	Longitudinal NS
3	3.11	0.0032	Transversal EW
4	11	0.0083	Vertical Z
5	7.17	0.0070	Longitudinal NS
6	7.01	0.0059	Transversal EW

Table 11S- Modals frequencies and amplitudes peaks identified for the sensor C11.

Mode	Frequencies / Hz	Amplitude peaks	Directions
1	2.94	0.020	Vertical Z
2	2.88	0.043	Longitudinal NS
3	2.96	0.025	Transversal EW
4	7.38	0.024	Transversal EW

Table 12S- Modals frequencies and amplitudes peaks identified for the sensor C12.

Mode	Frequencies / Hz	Amplitude peaks	Directions
1	2.88	0.039	Vertical Z
2	2.94	0.118	Longitudinal NS
3	2.88	0.149	Transversal EW
4	8.39	0.0295	Longitudinal NS
5	8.49	0.04216	Transversal EW

Table 13S- Modals frequencies and amplitudes peaks identified for the sensor C13.

Mode	Frequencies / Hz	Amplitude peaks	Directions
1	2.88	0.0446	Vertical Z
2	2.91	0.318	Longitudinal NS
3	2.88	0.3088	Transversal EW
4	8.79	0.0429	Longitudinal NS
5	8.76	0.0529	Transversal EW

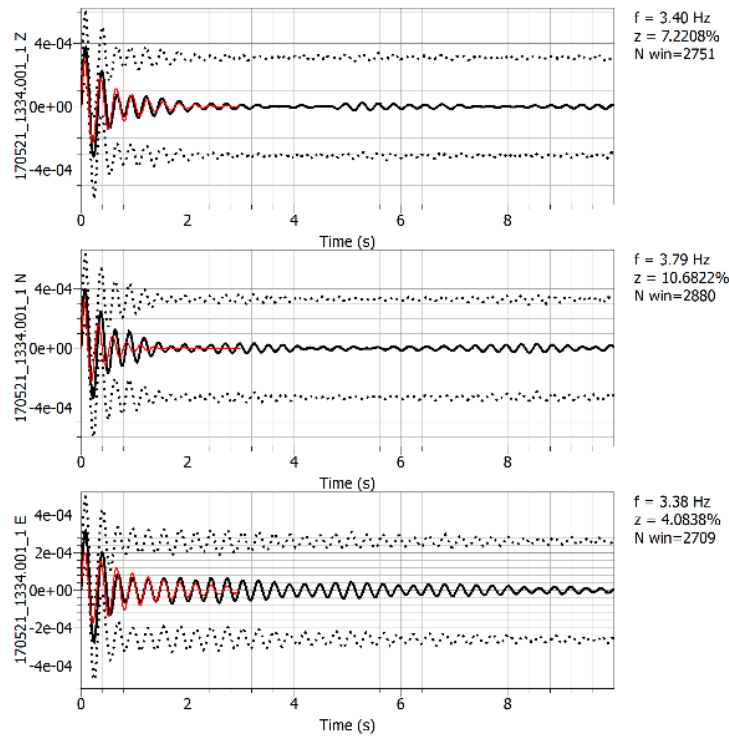


Figure 3S- Values of the damping coefficient at the recording point C1.

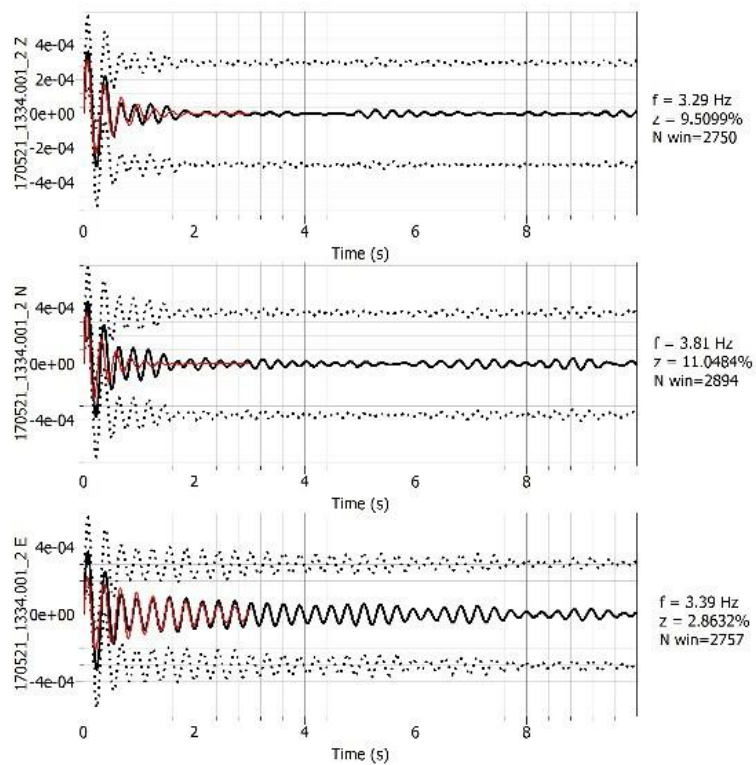


Figure 4S- Values of the damping coefficient at the recording point C2 between 2 Hz - 4 Hz.

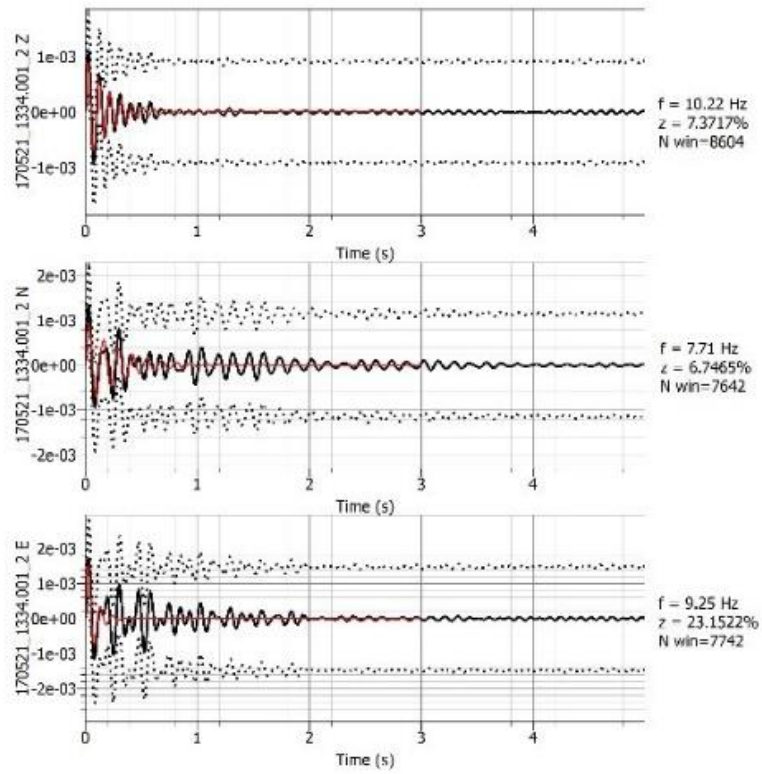


Figure 5S- Values of the damping coefficient at the recording point C2 between 6 Hz - 12 Hz.

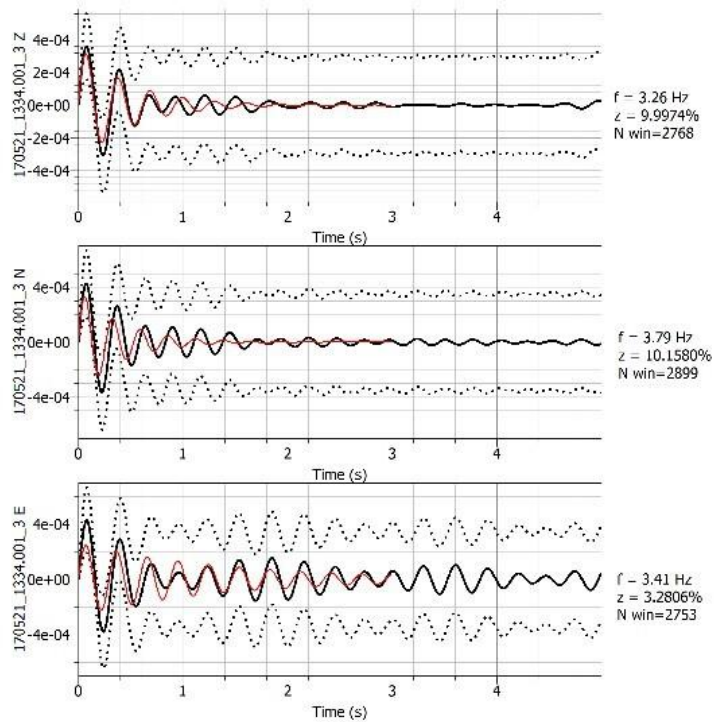


Figure 6S- Values of the e damping coefficient at the recording point C3 between 2 Hz- 4 Hz.

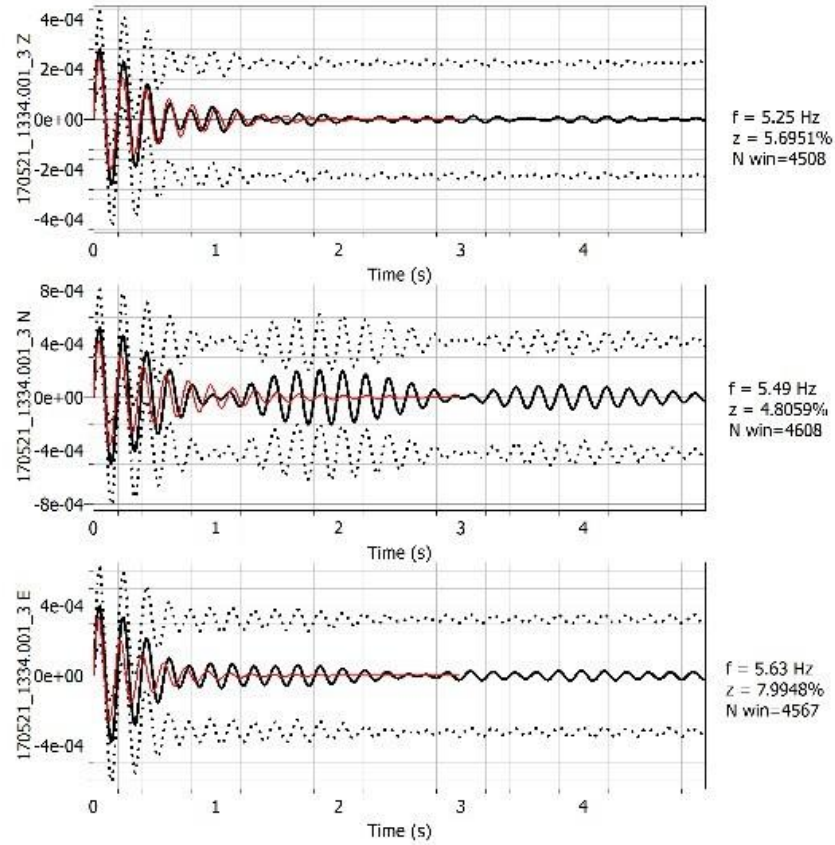


Figure 7S- Values of the e damping coefficient at the recording point C3 between 4 Hz- 6 Hz.

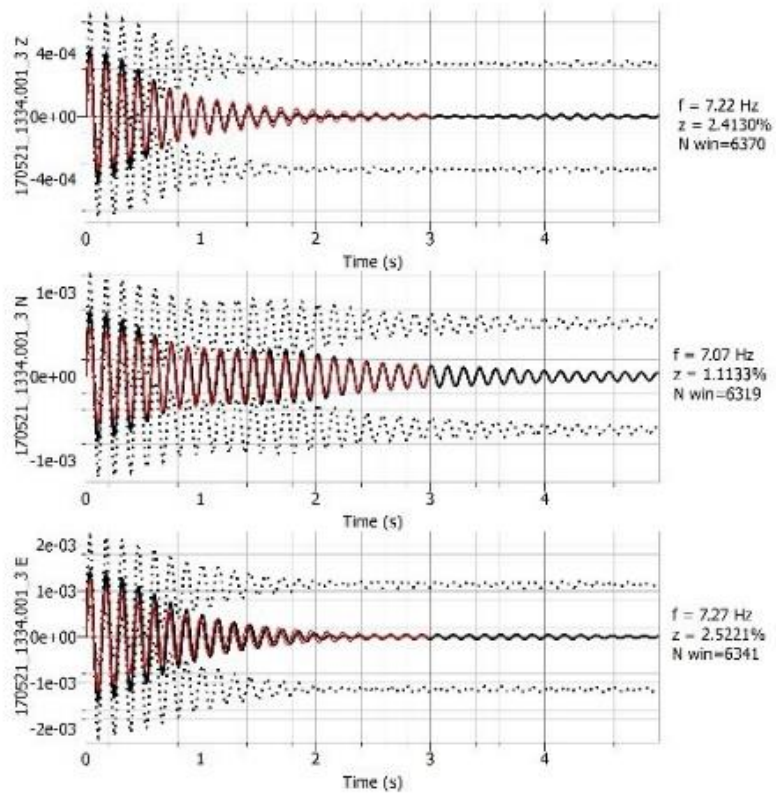


Figure 8S- Values of the e damping coefficient at the recording point C3 between 6 Hz- 8 Hz.

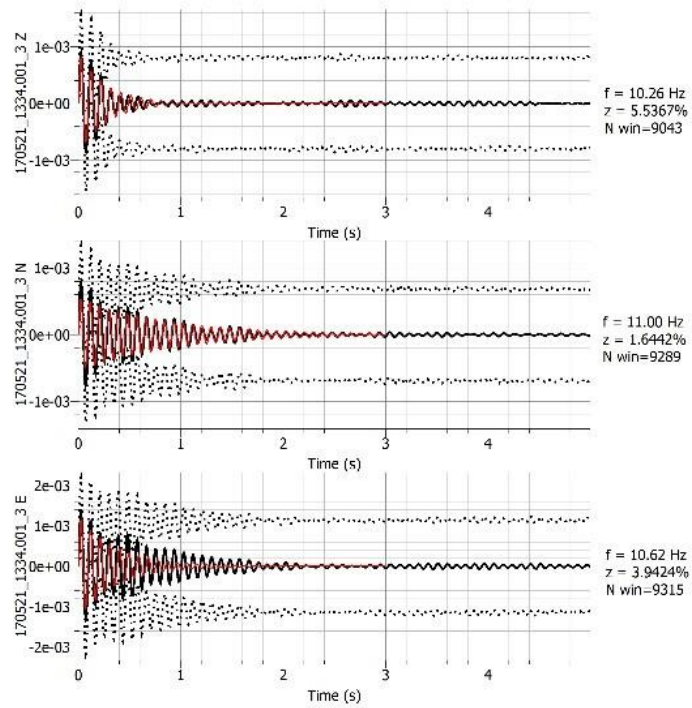


Figure 9S-Values of the e damping coefficient at the recording point C3 between 8 Hz- 12 Hz.

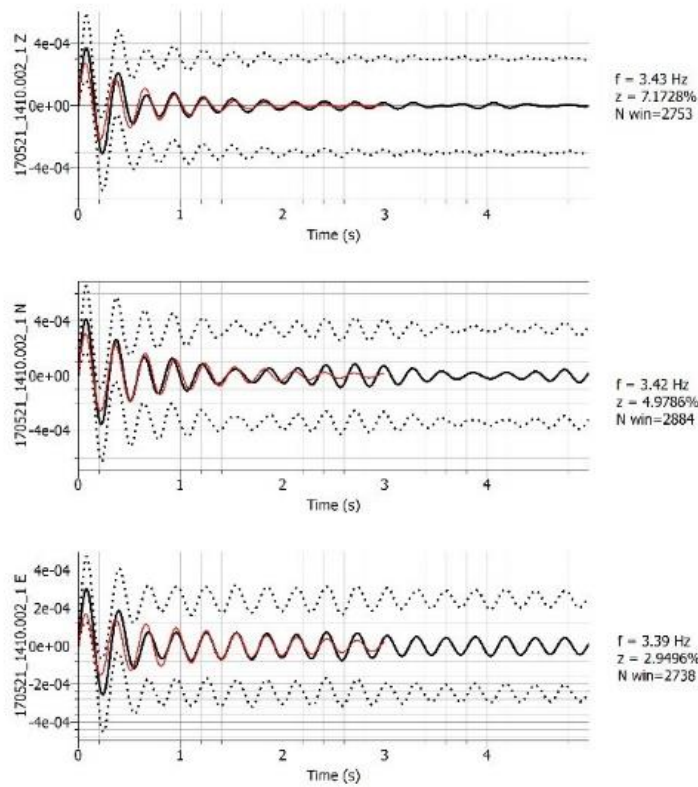


Figure 10S- Values of the damping coefficient at the recording point C4.

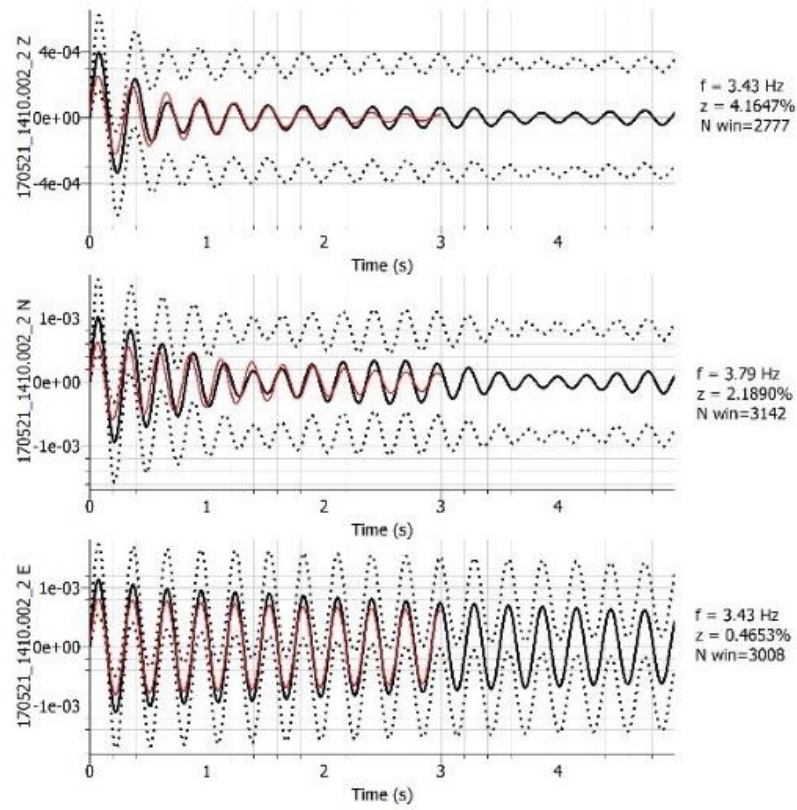


Figure 11S- Values of the damping coefficient at the recording point C5 between 2 Hz - 4 Hz.

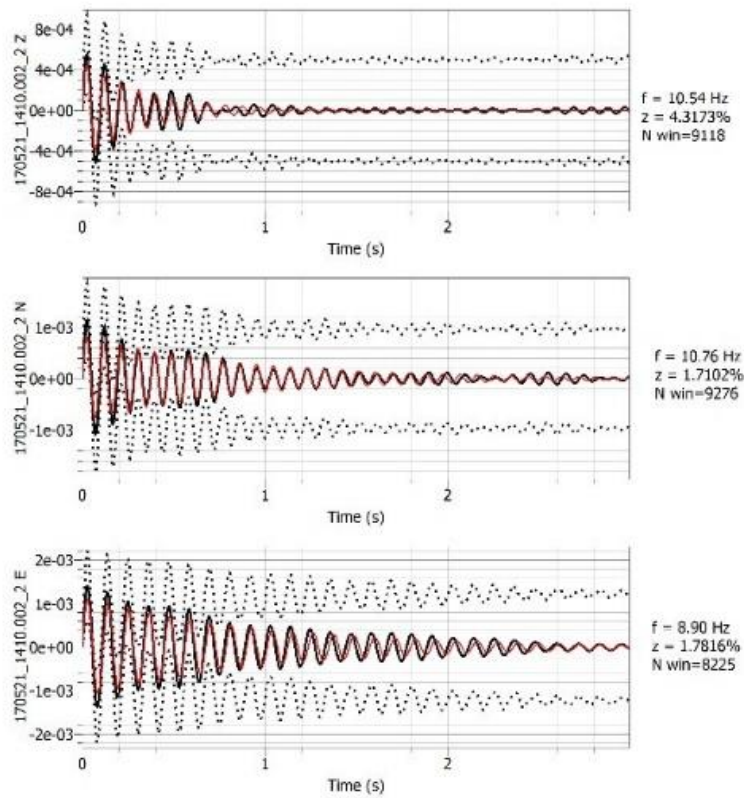


Figure 12S- Values of the damping coefficient at the recording point C5 between 8 Hz - 12 Hz.

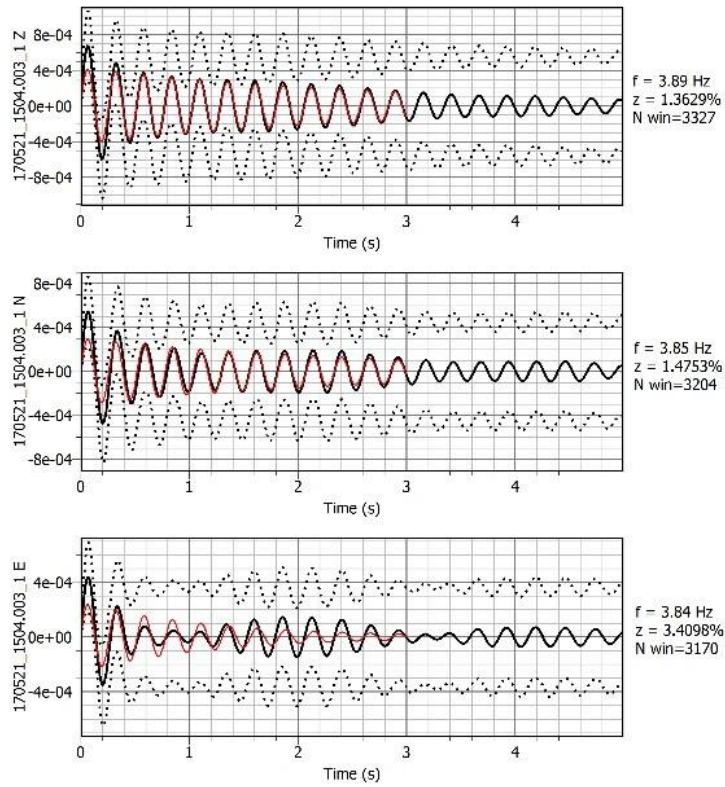


Figure 13S- Values of the damping coefficient at the recording point C6.

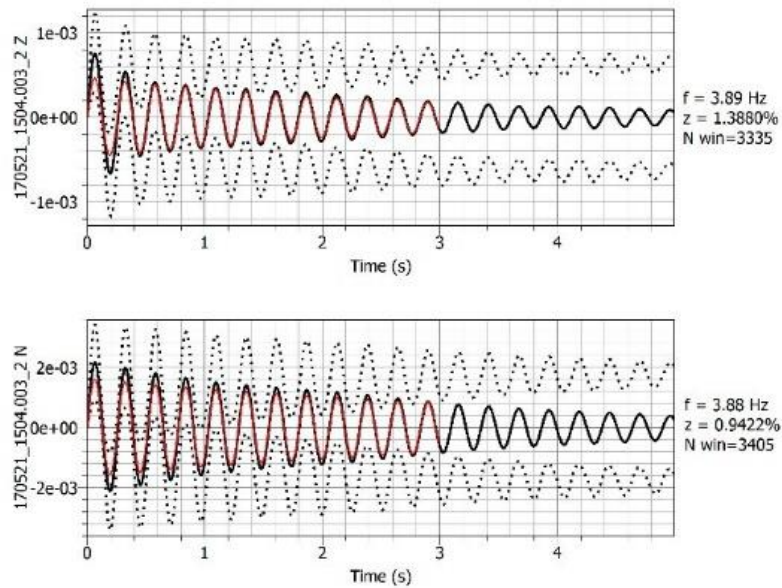


Figure 14S- Values of the damping coefficient at the recording point C7.

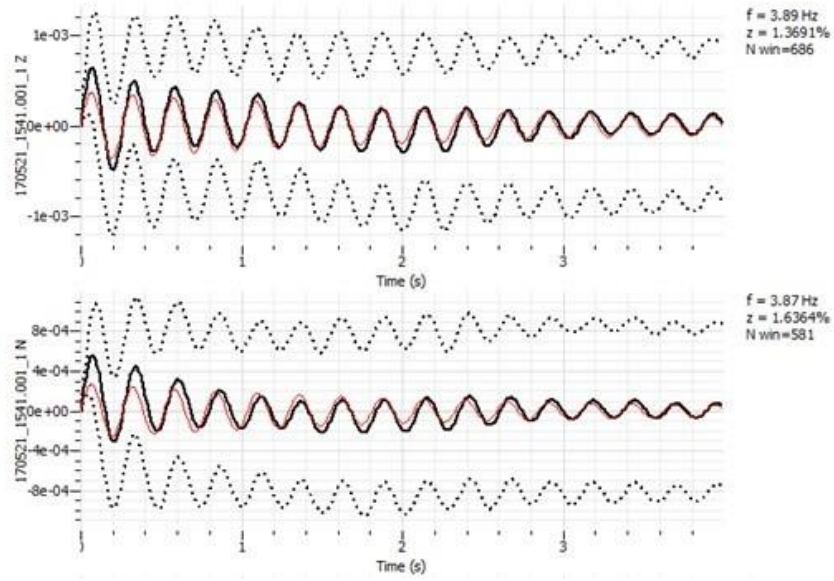


Figure 15S- Values of the damping coefficient at the recording point C8.

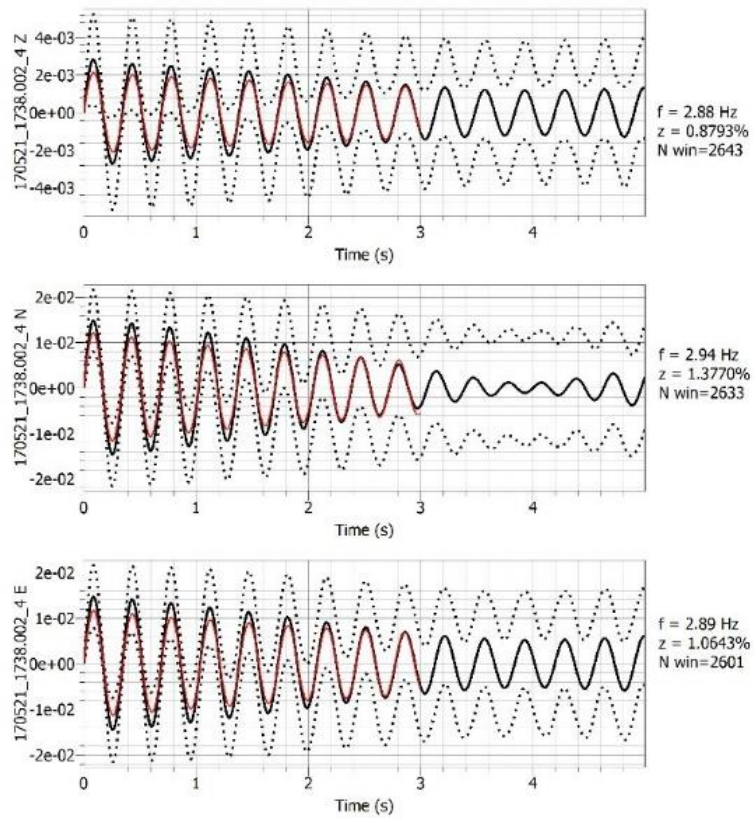


Figure 16S-Values of the damping coefficient at the recording point C9 between 2 Hz-3 Hz.

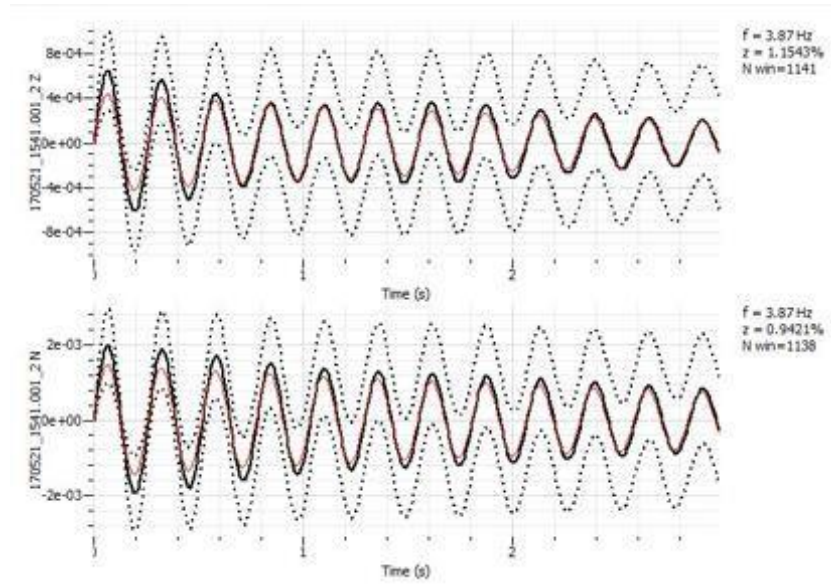


Figure 17S- Values of the damping coefficient at the recording point C9 between 3 Hz-4 Hz.

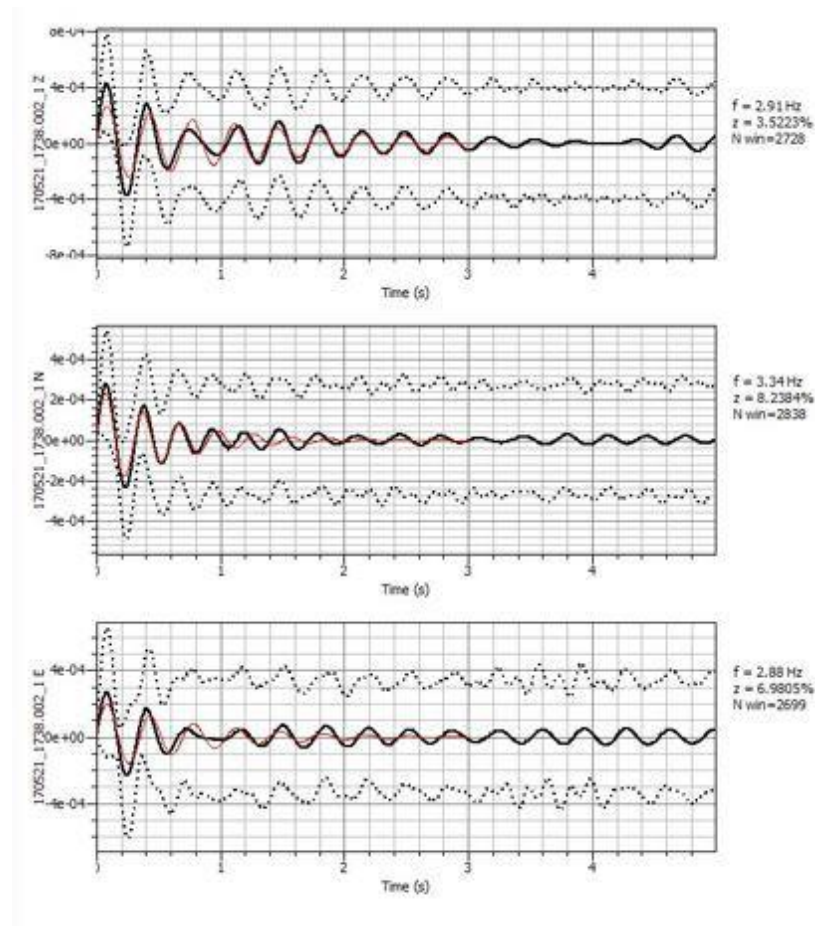


Figure 18S- Values of the minaret damping coefficient at the recording point C10.

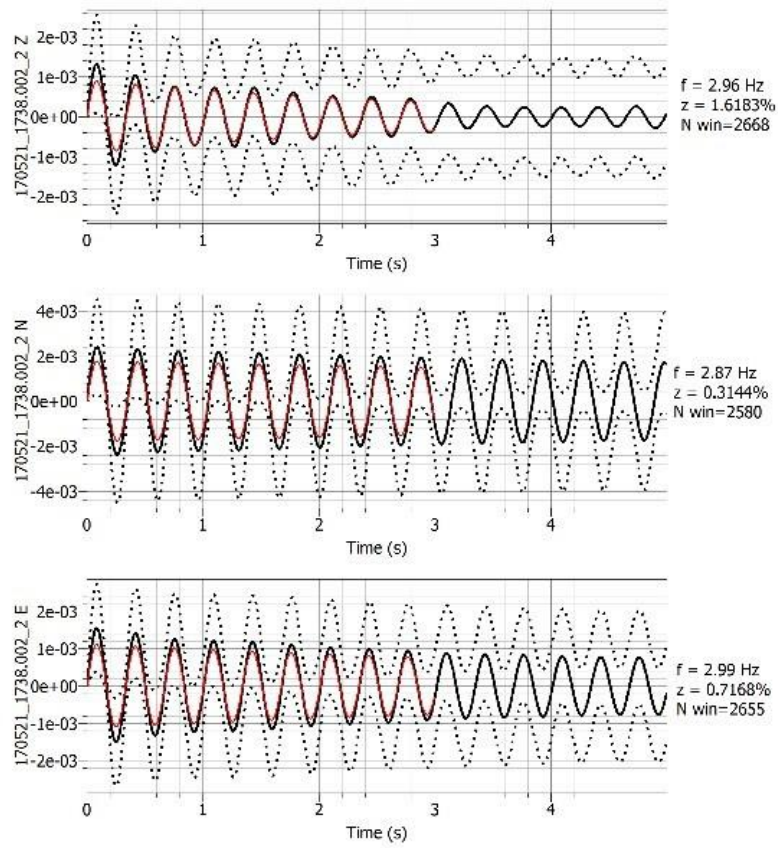


Figure 19S- Values of the minaret damping coefficient at the recording point C11.

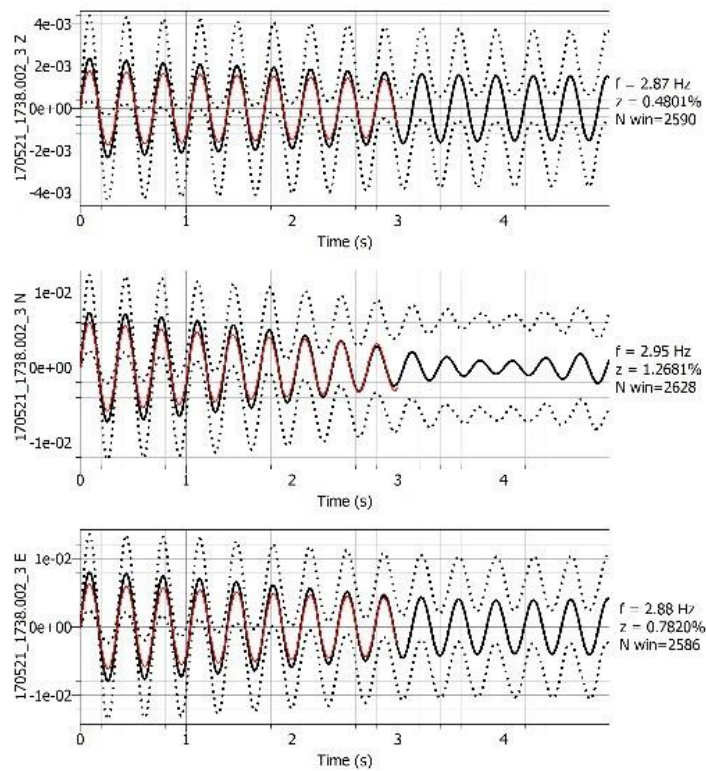


Figure 20S- Values of the minaret damping coefficient at the recording point C12.

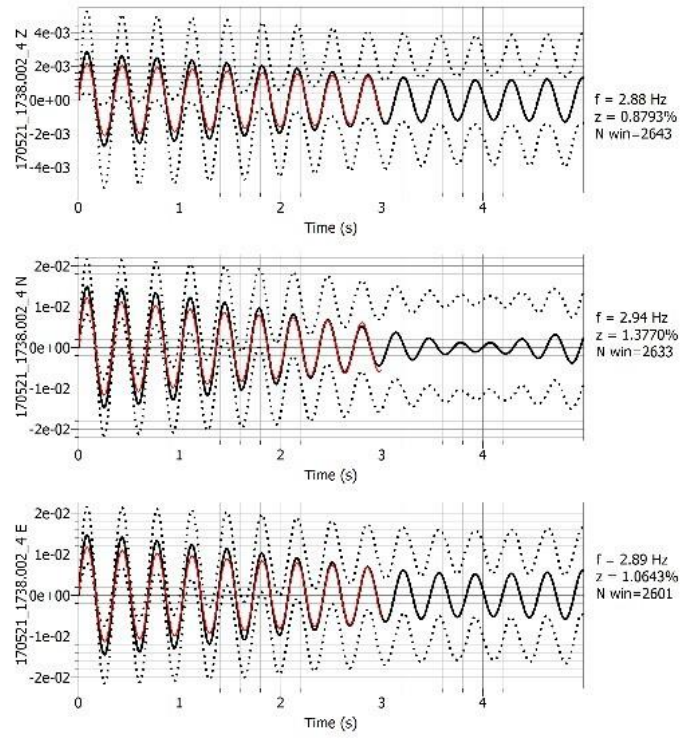


Figure 21S- Values of the minaret damping coefficient at the recording point C13.